

Simulation of anomalous Hall effect in ultracold gases

O. Dutta^{1,*}, A. Przysiężna^{2,3}, and J. Zakrzewski^{1,4}

¹ *Instytut Fizyki imienia Mariana Smoluchowskiego, Uniwersytet Jagielloński, ulica Reymonta 4, PL-30-059 Kraków, Poland*

² *Institute of Theoretical Physics and Astrophysics, University of Gdańsk, Wita Stwosza 57, 80-952 Gdańsk, Poland*

³ *National Quantum Information Centre of Gdańsk, Andersa 27, 81-824 Sopot, Poland*

⁴ *Mark Kac Complex Systems Research Center, Uniwersytet Jagielloński, Kraków, Poland*

(Dated: December 6, 2024)

We study ultracold fermions trapped in a shaken two dimensional triangular lattice. We find that, a combination of interaction induced tunneling and shaking can result in an emergent Dice lattice along with controllable staggered magnetic flux and synthetic non-Abelian fields. Moreover, by tuning the staggered flux, we show that one can enter the regime of Quantum Anomalous Hall effect. Our results are reminiscent of Anomalous Hall conductivity in spin-orbit coupled Ferromagnets.

PACS numbers: 67.85.Lm, 03.75.Lm, 73.43.-f

In many branches of quantum engineering special attention is paid to the creation of synthetic gauge fields [1–6] that can allow to study various condensed matter phenomena. A natural extension aims at creation of non-Abelian gauge fields [7–11] which can be then used to tune the band structure of the particles in the system. In particular, when the Berry curvature (a quantity connected to the geometric property of the band structure) is changed, exotic topological effects may be obtained [12]. For example, presence of local Berry curvature in spin-orbit coupled ferromagnets gives rise to Anomalous Hall conductivity [13–15]. Analogue of such effect is also proposed to appear in photonic lattices [16].

In this paper we focus on the systems of ultracold gases that provide versatile platform to simulate and engineer novel forms of matter. Our proposal consists of attractive two-species fermions (as in [17]) trapped in a periodically shaken triangular lattice. The triangular lattice introduces geometrical frustration while the shaking can resonantly enhance the interaction-induced sp -orbital tunneling. In effect, an emergent Dice lattice is formed accompanied by a strong staggered flux. Moreover, inclusion of p -orbitals leads to formation of synthetic non-Abelian fields. The system shows spontaneous magnetization accompanied by appearance of anomalous Hall conductivity forming an ultracold gas analogue of spin-orbit coupled ferromagnetic insulators [14, 15]. Furthermore, we show that, in presence of a strong staggered field, one can reach the regime of quantized Hall conductivity.

Model : Consider an unequal mixture of two-species attractive ultracold fermions (denoted by \uparrow, \downarrow) trapped in a triangular lattice with fillings $n^\uparrow = 1/3$ and $n^\downarrow > 1/3$. Strong attractive contact interaction between atoms leads to pairing – formation of composites between the \uparrow and \downarrow -fermions, as studied experimentally for different lattice geometries [18–20]. We define a composite creation operator $\hat{c}_i^\dagger = \hat{s}_i^\dagger \hat{s}_{i1}^\dagger$ with the corresponding number operator $\hat{n}_i^c = \hat{c}_i^\dagger \hat{c}_i$. $\hat{s}_{\sigma i}^\dagger, \hat{s}_{\sigma i}$ are the creation and annihilation operators of the σ fermions in the respective s -bands. The composites are hardcore bosons which anti-commute

at the same site, $\{\hat{c}_i, \hat{c}_i^\dagger\} = 1$, and commute for different sites, $[\hat{c}_i, \hat{c}_j^\dagger] = 0$ for $i \neq j$ [21].

Using lattice shaking technique we tune the standard intra-band tunneling to negligible values [22–24]. Such shaking simultaneously makes the intra-band interaction induced tunneling [25–30] (called also bond-charge tunneling) vanishingly small. The only remaining tunneling mechanism is then the sp -hybridized inter-band interaction induced tunneling [17] which can be resonantly enhanced adjusting the shaking frequency. Then the system at low-energies consists of the composites and the excess \downarrow -fermions with filling $n^\downarrow - n^\uparrow$ (note that the \downarrow - or \uparrow -fermions of the composites can not undergo sp -tunneling without breaking the strong pairing - this costs energy). Thus, the low-energy local Hilbert subspace is spanned by $\hat{c}_i^\dagger|0\rangle, \hat{p}_{\pm, i}^\dagger \hat{c}_i^\dagger|0\rangle$, and $\hat{s}_i^\dagger|0\rangle$ states, where $\hat{s}_i, \hat{p}_{\pm, i}$ denote the excess \downarrow -fermions operators in the s - and p -orbitals. The latter are written in the chiral representation $\hat{p}_\pm = (\hat{p}_x \pm i\hat{p}_y)/\sqrt{2}$. Within this subspace, one can show that the composite number operator equals the \uparrow -fermions number operator, $\hat{n}_i^c = \hat{n}_i^\uparrow$ and the densities $n^c = n^\uparrow = 1/3$. Other important relations are: i) $\hat{s}_i^\dagger \hat{c}_i^\dagger = 0$ – a composite and an excess s -fermion can not occupy the same site due to the Pauli-exclusion principle; ii) $[\hat{n}_i^c, \hat{p}_{\pm, j}] = 0$, and iii) $[\hat{n}_i^c, \hat{s}_j] = 0$ for $i \neq j$.

Therefore, an effective Hamiltonian for the composites and the excess \downarrow -fermions consists of three parts [31]: H_{sp} describing interaction-induced sp -tunneling, H_{int} describing interactions, and $H_{shaking}$ describing driving force. First of them reads,

$$\frac{H_{sp}}{J_{sp}} = \frac{1}{\sqrt{2}} \sum_{i, \delta, \sigma = \pm} f_{\delta\sigma} \hat{p}_{\sigma, i}^\dagger \hat{n}_i^c \hat{s}_{i+\delta} + h.c., \quad (1)$$

where vectors connecting nearest-neighbors are $\delta = \pm\delta_0, \pm\delta_\pm$ with $\delta_0 = (1, 0), \delta_+ = (1/2, \sqrt{3}/2), \delta_- = (1/2, -\sqrt{3}/2)$. Due to the angles created by the different δ vectors, in the chiral representation an additional phase factor f_δ appears. In the harmonic approximation of the triangular lattice potential, this phase factor

is given by $f_{\delta\sigma} = \exp[-i\sigma \tan^{-1}(\delta_y/\delta_x)]$. The tunneling J_{sp} is given in terms of the s - and p -band Wannier functions $W_{00}^i(x, y)$ and $W_{10}^i(x, y)$ as

$$J_{sp} = g_{2D} \int \int W_{10}^i(x, y) (W_{00}^i(x, y))^2 W_{00}^{i+\delta_0}(x, y) dx dy, \quad (2)$$

with the contact interaction strength g_{2D} adjusted for a quasi-2D geometry (with a tight harmonic confinement along z) [32]. The second part is the interaction Hamiltonian including higher band contribution. It reads [17],

$$H_{\text{int}} = U_2 \sum_{\mathbf{i}} \hat{n}_i^c + U_{sp} \sum_{\mathbf{i}, \sigma=\pm} \hat{n}_i^c \hat{n}_{\sigma\mathbf{i}} + E_1 \sum_{\mathbf{i}, \sigma=\pm} \hat{n}_{\sigma\mathbf{i}}, \quad (3)$$

where U_2 denotes the energy of the composites and U_{sp} is the additional interaction energy to occupy the p -orbital of a composite filled site. E_1 is the single-particle excitation energy of the p -band. Shaking with elliptical periodic driving force leads to [23],

$$H_{\text{shaking}} = \sum_{\mathbf{i}} \mathbf{i} \cdot \mathbf{F}_t (\hat{n}_{\sigma\mathbf{i}} + \hat{n}_{+\mathbf{i}} + \hat{n}_{-\mathbf{i}}),$$

with the shaking force $\mathbf{F}_t = [-K_1 \sin(\Omega t) \hat{x} + K_2 \cos(\Omega t + \Phi) \hat{y}]$. We consider the case where $J_{sp} \ll U_2, U_{sp} \leq \Omega$. That allows us to use rotating-wave approximation and Floquet theorem and average the terms fast oscillating in time [31].

The sp -tunneling will be resonantly enhanced when the energy to occupy the p -bands is an integer multiple of the shaking frequency. This translates into the condition that $E_1 + U_{sp} = N\Omega$ for integer N . The resonance order, N , can be controlled by varying either the lattice depth, interaction strength or the driving frequency. The time-averaged Hamiltonian then becomes,

$$\frac{H_{\text{avg}}}{J_{sp}} = \frac{1}{\sqrt{2}} \sum_{\mathbf{i}, \delta, \sigma=\pm} F_{\delta} f_{\delta} \hat{p}_{\sigma, \mathbf{i}}^{\dagger} \hat{n}_i^c \hat{s}_{\mathbf{i}+\delta}, \quad (4)$$

where

$$F_{\delta} = \frac{1}{2\pi} \int_0^{2\pi} \exp[iN\Omega t - iK_{\delta} \cos(t + \alpha_{\delta})] dt \\ = \mathcal{J}_N(K_{\delta}/\Omega) \exp[-iN\alpha_{\delta}], \quad (5)$$

with $\mathcal{J}_N(x)$ being the Bessel function of the first kind with integer order N . The amplitudes are $K_{\delta_0} = K_1$ and $K_{\delta_{\pm}} = [K_1^2 + 3K_2^2 \pm 2\sqrt{3}K_1K_2 \sin \Phi]^{1/2}$. The phase factor $\alpha_{\delta} = 0$ for $\delta = \pm\delta_0$ and $\alpha_{\delta} = \tan^{-1} \left[\frac{\sqrt{3} \cos \Phi}{1 \pm \sqrt{3} \sin \Phi} \right]$ for $\delta = \pm\delta_{\pm}$. Moreover, lattice shaking also induces phases to the sp -tunnelings (5) as illustrated in Fig.1(a) (see also [31]).

Ground state composite structure: The composite number operator \hat{n}_i^c commutes with the Hamiltonian (4), $[\hat{n}_i^c, \hat{H}_{\text{avg}}] = 0$. Therefore, we can characterize a site by the presence or the absence of a composite, i.e. $n_i^c = 1, 0$ which makes the Hamiltonian, (4), quadratic in operators

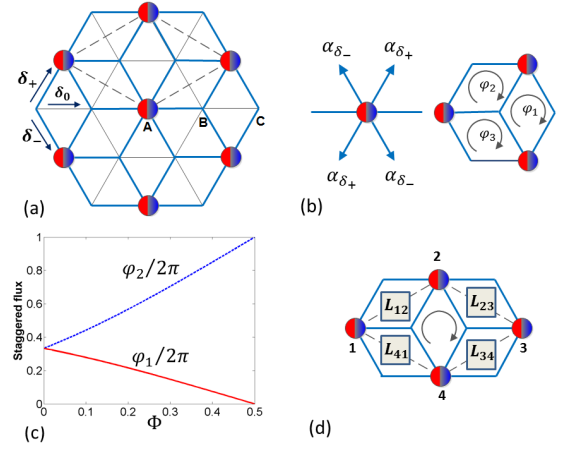


FIG. 1. (a) The representation of the system considered in the paper. Red-and-blue spheres refer to the composites. The thin lines denote the bonds in the original triangular lattice and the blue lines represent the bonds for the excess \downarrow -fermions in the emerged dice lattice. On the composite occupied sites we have p -orbitals for the excess fermions while on vacant sites we have s -orbitals for the excess fermions. δ_0, δ_{\pm} correspond to the vectors connecting the nearest neighbors and the sites **A**, **B**, **C** symbolize the basis for the dice lattice. (b) Left panel: The tunneling phases described in Eq.(5). Right panel: Three elementary cells present in the dice lattice and the corresponding fluxes in those cells. The arrows show the direction along which the fluxes are calculated. (c) The magnitude of the fluxes in each cell plotted as a function of the shaking phase Φ (in the units of π). (d) The elementary plaquette for the A sites in the dice lattice along with the matrices L_{ll+1} coupling the sites l and $l+1$.

for a particular realization of composite configuration. The ground state structure of the system is given by the configuration which minimizes the kinetic energy or maximizes the delocalization area of the excess \downarrow -fermions. To gain an intuitive understanding of the ground state structure of the composites, consider first a composite at some chosen site A . The energy is minimized when all the neighboring sites (forming hexagon with the site A in the center) are without composites. This facilitates the sp tunneling from a p orbital at site A to the neighboring sites. Any composite on these neighboring sites increases the energy by $J_{sp} F_{\text{avg}, \delta}$. Thus, for a composite filling of $n^c = 1/3$, the delocalization area is maximized by filling the lattice with hexagons with a composite at their center. We have verified that this indeed is the ground state structure carrying out Simulated Annealing (described in [17]) on small systems. The resulting self-organized structure for a lattice is known as a Dice lattice (Fig. 1(a)). Its basis consists of three sites denoted A, B and C . The A site consists of two orbitals p_+ and p_- whereas the site B and C have only s -orbitals. The basis vectors for the Dice lattice are given by $\mathbf{a}_1 = (3/2, \sqrt{3}/2)$ and $\mathbf{a}_2 = (3/2, -\sqrt{3}/2)$. For any deviation from the $1/3$ filling of the composites, the excess composites or va-

cancies will show up as impurities on top of the Dice lattice as long as the density of such impurities is small ($n_{\text{imp}} \ll 1/3$).

Creation of a staggered field : For the Dice lattice, one can construct three different plaquettes as shown in Fig. 1(b). Phases of the tunneling amplitudes induce fluxes due to Aharnov-Bohm effect in each of those plaquettes [denoted by φ_1, φ_2 and φ_3 , see Fig.1(b) and calculated along the direction of the arrow]. The induced flux is staggered in nature as the phases obey the constraint $\text{mod}(\varphi_1 + \varphi_2 + \varphi_3, 2\pi) = 0$. Fig. 1(c) shows the flux strengths for $N = 1$. In particular, for $\Phi = 0$, $\varphi_1 = \varphi_2 = \varphi_3 = 2\pi/3$ which is equivalent to a uniform magnetic flux of the same magnitude. With growing Φ , fluxes change with all fluxes vanishing at $\Phi = \pi/2$.

Non-Abelian nature: The primary plaquette involving the p -orbitals is given by the parallelogram shown in Fig. 1(d). An effective kinetic energy term around the plaquette for the A sites may be written as

$$\frac{H_{\text{kin},A}}{J_{\text{sp}}} = \Psi_2^\dagger L_{12} \Psi_1 + \Psi_3^\dagger L_{23} \Psi_2 + \Psi_4^\dagger L_{34} \Psi_3 + \Psi_1^\dagger L_{41} \Psi_4 + h.c. \quad (6)$$

where the array $\Psi_l = (p_+, p_-)_l$ denotes p -orbitals at site l . The corresponding link variables connecting the neighboring A sites along the clockwise direction are given by 2×2 matrix L_{mn} with

$$L_{12} = \begin{pmatrix} \cos(\pi/3 + \alpha_{\delta_-}) & e^{i\pi/3} \cos \alpha_{\delta_-} \\ e^{-i\pi/3} \cos \alpha_{\delta_-} & \cos(\pi/3 - \alpha_{\delta_-}) \end{pmatrix}. \quad (7)$$

L_{23} is given by changing $\pi/3 \rightarrow -\pi/3$ and $\delta_- \rightarrow \delta_+$ in the expression for L_{12} in Eq.(7). Moreover, we find that $L_{12} = L_{34}$ and $L_{23} = L_{41}$ and they depend on the staggered flux through the phase of the tunneling amplitudes. Moreover, the link variables are not unitary, which makes it not straightforward to describe them as synthetic non-Abelian fields. Nonetheless one can polar decompose them into unitary part, $L_{mn} = \mathcal{S}_{mn} \mathcal{U}_{mn}$, where $\mathcal{U}_{mn}^\dagger \mathcal{U}_{mn} = 1$. Then one can define a corresponding Wilson loop parameter [33]

$$W = \text{Tr} [\mathcal{U}_{12} \mathcal{U}_{23} \mathcal{U}_{34} \mathcal{U}_{41}].$$

The Wilson loop parameter has (i) an intrinsic contribution due to the appearance of sp -band tunneling and (ii) an extrinsic contribution due to the external staggered flux induced by shaking. As a result, the link matrices are of non-Abelian nature ($W \neq 2$) for any shaking phase Φ .

Results: First, we study the behavior of the system in the absence of staggered flux realized for $N = 1$, $\Phi = \pi/2$ Fig. (1). The effective non-Abelian field is intrinsic in nature and the corresponding dispersion relation for the lowest energy band is shown in Fig. 2a. The main characteristic of the dispersion relation is the appearance of two non-equivalent Dirac cones and disappearance of flat

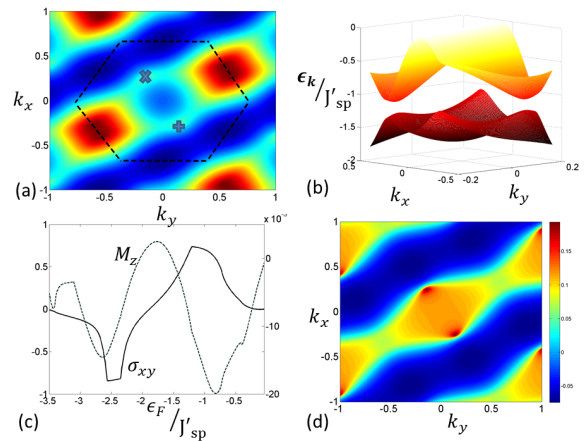


FIG. 2. (a) The dispersion relation for the lowest energy band as a function of a lattice momentum \mathbf{k} for zero staggered flux, $\varphi_1 = \varphi_2 = \varphi_3 = 0$ corresponding to shaking phase $\Phi = \pi/2$ and $N = 1$. The dark blue part denotes low energy regions. The \times and $+$ denote positions of Dirac points. (b) The dispersion $\epsilon_{\mathbf{k}}$ for the first two band in the presence of small staggered flux for $\Phi = \pi/4$. The presence of the staggered flux along with the non-Abelian nature of the system helps to open a gap near the Dirac points. The tunneling strength is given by $J'_{sp} = J_{sp} J_1(K_1/\Omega)$. (c) The magnetization (8) and Hall conductivity as a function of Fermi energy for $\Phi = \pi/4$ and $N = 1$. Spontaneous magnetization appears due to time-reversal symmetry breaking. Local Berry curvature results in a finite Hall conductivity which shows plateau like structure due to the presence of the gap between the first two bands. (d) The magnetization in momentum space as a function of crystal momentum \mathbf{k} shows sharp peaks near the two Dirac points for $\Phi = \pi/4$ and $N = 1$. They correspond to the presence of monopole like structure in the corresponding Berry phase.

bands. This is in contrast to the dispersion relation in a normal Dice lattice without intrinsic non-Abelian contribution where the dispersion relation contains an intersection Dirac cone and a flat band. Moreover, above a certain Fermi energy (of the excess fermions), the first two bands are degenerate. When we introduce the staggered flux, the dispersion changes and the gap opens at the band touching points (Fig. 2b). Once the Fermi energy is higher than the gap, the two bands become degenerate again. This is in a stark contrast to other situations with nearest neighbor tunneling where staggered flux leads only to the movement of the Dirac cones [34, 35] and to opening a gap one either needs long-distance tunneling [10, 36], uniform magnetic field or synthetic non-Abelian fields along with magnetic field [37].

Anomalous Hall effect: Consider the local magnetization (\mathcal{M}_z) in position space as well as magnetization in momentum space defined as

$$\begin{aligned} \mathcal{M}_z &= \langle \hat{n}_{i+} \rangle - \langle \hat{n}_{i-} \rangle, \\ \mathcal{M}_{\mathbf{k}} &= \langle \hat{n}_{\mathbf{k}+} \rangle - \langle \hat{n}_{\mathbf{k}-} \rangle. \end{aligned} \quad (8)$$

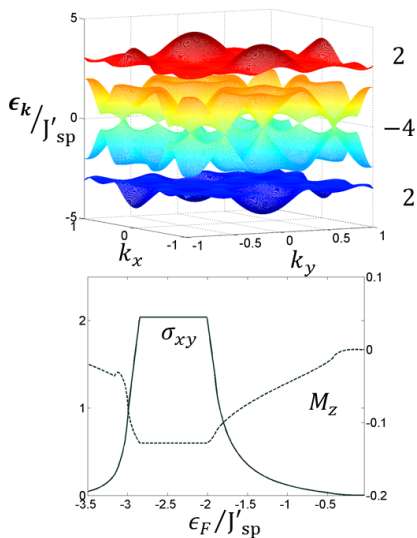


FIG. 3. The dispersion relation for $\Phi = 0$ which corresponds to staggered flux with $\varphi_1 = \varphi_2 = 2\pi/3$ and $N = 1$. The numbers on the right hand side of the figure show the invariant Chern numbers corresponding to the respective bands. Bottom plot represents the Hall conductivity σ_{xy} and the magnetization M_z for that case.

A non-zero local magnetization characterizes the breaking of time-reversal symmetry as the particles acquire local angular momentum due to the particle number difference between the p_+ and p_- orbitals. First, we find that the presence of non-zero staggered flux immediately results in non-zero M_z and in opening of the gap. Thus, appearance of non-zero M_z can be used as an indirect evidence for the presence of a gap in our system. The local magnetization is shown in Fig.2c (dashed line) for a small staggered flux. It vanishes only when the first two bands are totally filled. The presence of spontaneous magnetization (spontaneous time-reversal symmetry breaking) is reminiscent of spin-orbit coupled ferromagnets [13]. Moreover, to look into the topological nature of the system, we define the intrinsic Hall conductivity,

$$\sigma_{xy}^n = \int_{BZ} \Omega_n(\mathbf{k}) d\mathbf{k} / 2\pi.$$

The Berry curvature, $\Omega_n(\mathbf{k})$, for the n -th band is given by $\Omega_n(\mathbf{k}) = \nabla_{\mathbf{k}} \times \langle u_{n\mathbf{q}} | \nabla_{\mathbf{k}} | u_{n\mathbf{q}} \rangle$ where $|u_{n\mathbf{q}}\rangle$ denotes an eigenvector for the n -th band. The total Hall conductivity then depends on the Fermi energy ϵ_F of the system and is given by $\sigma_{xy} = \sum_{\epsilon_n < \epsilon_F} \sigma_{xy}^n$ [Fig.2c (solid line)]. We find that the local Berry curvature is concentrated near the Dirac points which results in a non-zero contribution to σ_{xy}^n when ϵ_F is in the band. As ϵ_F enters the band gap, we find that σ_{xy}^n flattens at a value $> 1/2$. This can be ascribed to the presence of two Dirac cones near the band gap. As we increase ϵ_F , the contribution from the next band begins to play a role and eventually

the conductivity changes sign. The second peak appears when the Fermi energy reaches the maximum of the first band. Such structures in conductivity have been predicted to arise due to the presence of magnetic monopoles in the momentum space [38].

Quantum Anomalous Hall effect: Finally, consider the strong flux limit, e.g the case of $\Phi = 0$ where the flux through each plaquette is $2\pi/3$. Strong flux results in lifting the degeneracy between the first two bands (Fig. 3, top plot). The middle two bands still touch each other in the form of Dirac cones. With the degeneracy lifted, one can define Chern numbers given by $\nu = (2, -4, 2)$ resulting in the appearance of Quantum Anomalous Hall effect. We have also calculated the Hall conductivity and when the Fermi energy of the excess fermions resides in the band gap, conductivity becomes integer valued (Fig. 3, bottom plot). The magnitude of the band gap is $\approx J_{sp}$. For a triangular lattice (lattice constant $a = 500\text{nm}$) with lattice depth of $6E_R$ and transverse frequency of $10E_R$, the sp tunneling strength in the harmonic approximation is given by $J_{sp} \sim 0.008E_R$ assuming the scattering length of ~ 400 Bohr radius. This corresponds to a band gap of about ~ 10 nano-Kelvin which determines the temperature regime where the Hall phase can be observed. For the Dice lattice with dilute impurities, the Hall conductivity presented in this paper remain unchanged due to the topological nature of the Berry curvature for the dispersion bands [13]. The band topology discussed here can be measured in principle by using recently proposed methods of Ramsey interferometry and Bloch oscillations [39, 40], or from momentum distribution from Time-of-Flight images [41]. Moreover, the generation of local orbital angular momentum due to broken time-reversal symmetry in the chiral p -orbitals can also be detected by time-of-flight measurements [42].

Conclusions: To summarize, we considered an unequal mixture of attractively interacting fermions in a shaken triangular lattice. Pairing produces immobile composites that gives rise to Dice lattice for the excess fermions. Adjustments of shaking frequency and amplitude allow to make intra-band tunnelings negligible while resonantly enhancing interaction-induced sp -tunnelings for the excess fermions. Moreover, shaking leads to the controlled staggered magnetic field and induces (on the p -orbitals) non-Abelian character of the system. Their joint effect leads to spontaneous chiral magnetization (due to time reversal symmetry breaking) along with appearance of Anomalous Hall effect. Many fascinating questions related to the findings here can be investigated further including the role of impurities, long-range interaction etc. Moreover, by using dipolar atoms, one can further study many-body effects like superconductivity [43, 44], density-waves in presence of the artificial non-abelian gauge fields presented here.

We thank M. Lewenstein and K. Sacha for enlightening discussions. This work was realized under Na-

tional Science Center (Poland) project No. DEC-2012/04/A/ST2/00088. A.P. is supported by the International PhD Project "Physics of future quantum-based information technologies", grant MPD/2009-3/4 from Foundation for Polish Science and by the University of Gdansk grant BW 538-5400-B169-13-1E.

* E-mail: omjyoti@gmail.com

- [1] J. Dalibard, F. Gerbier, G. Juzeliunas, and P. Öhberg, *Rev. Mod. Phys.* **83**, 1523 (2011).
- [2] Y. J. Lin, R. L. Compton, K. Jimenez-Garcia, J. V. Porto, and I. B. Spielman, *Nature* **462**, 628 (2009).
- [3] M. Aidelsburger, M. Atala, S. Nascimbène, S. Trotzky, Y.-A. Chen, and I. Bloch *Phys. Rev. Lett.* **107**, 255301 (2011).
- [4] N. R. Cooper, *Phys. Rev. Lett.* **106**, 175301 (2011).
- [5] T. Uehlinger *et. al.* *Phys. Rev. Lett.* **111**, 185307 (2013)
- [6] K. Fan, Z. Yu and S. Fan, *Nature Photonics* **6**, 782 (2012)
- [7] M. Lewenstein, A. Sanpera, and V. Ahufinger, *Ultracold Atoms in Optical Lattices: Simulating quantum many-body systems*, Oxford University Press, London, (2012).
- [8] H. Terças, H. Flayac, D. D. Solnyshkov, and G. Malpuech *Phys. Rev. Lett.* **112**, 066402 (2014)
- [9] Y.-J. Lin, K. Jiménez-García, and I. B. Spielman, *Nature* **471**, 83-86 (2011).
- [10] P. Hauke, *et. al.*, *Phys. Rev. Lett.* **109**, 145301 (2012).
- [11] A. Kosior, K. Sacha, Arxiv: 1403.1221 (2014).
- [12] M. Z. Hassian and c. L. Kane, *Rev. Mod. Phys.* **82**, 3045 (2010).
- [13] N. Nagaosa, J. Sinova, S. Onoda, A. H. MacDonald, and N. P. Ong, *Rev. Mod. Phys.* **82**, 1539 (2010).
- [14] R. Yu, *et. al.*, *Science* **329**, 61 (2010).
- [15] C.-Z. Chang, *et. al.*, *Science* **340**, 167 (2013).
- [16] T. Ozawa, I. Carusotto, *Phys. Rev. Lett.* **112**, 133902 (2014).
- [17] O. Dutta, A. Przysiężna, and M. Lewenstein, *Phys. Rev. A* **89**, 043602 (2014).
- [18] J. K. Chin *et. al.*, *Nature* **443**, 961 (2006).
- [19] N. Strohmaier *et. al.*, *Phys. Rev. Lett.* **99**, 220601 (2007).
- [20] L. Hackermüller *et. al.*, *Science* **327**, 1621 (2010).
- [21] R. Micnas, J. Ranninger, and S. Robaszkiewicz, *Rev. Mod. Phys.* **62**, 113 (1990).
- [22] A. Eckardt, C. Weiss, and M. Holthaus, *Phys. Rev. Lett.* **95**, 260404 (2005),
- [23] J. Struck, *et. al.*, *Science* **333**, 996 (2011).
- [24] J. Struck, *et. al.*, *Nat. Phys.* **9**, 738 (2013).
- [25] J. E. Hirsch, *Physics C* **158**, 326 (1989).
- [26] T. S. Best *et. al.* *Phys. Rev. Lett.* **102**, 030408 (2009).
- [27] O. Dutta, A. Eckardt, P. Hauke, B. Malomed, and M. Lewenstein, *New. J. Phys.* **12**, 023019 (2011).
- [28] A. Mering and M. Fleischhauer, *Phys. Rev. A* **83**, 063630 (2011).
- [29] D.-S. Lühmann, O. Jürgensen, and K. Sengstock, *New. J. Phys.* **14**, 033021 (2012).
- [30] M. Łącki, F. Delande, and J. Zakrzewski, *New. J. Phys.* **15**, 013062 (2013).
- [31] See Supplementary Material for a more detailed description of various tunneling processes in the Hamiltonian and its time averaging.
- [32] D. S. Petrov, M. Holzmann, and G. V. Shlyapnikov, *Phys. Rev. Lett.* **84**, 2551 (2000).
- [33] C. Wetterich, Arxiv: 1307.0722 (2013).
- [34] L. Tarruell, *et. al.*, *Nature* **483**, 302 (2012).
- [35] L.-K. Lim, A. Hemmerich, and C. M. Smith, *Phys. Rev. A* **81**, 023404 (2010).
- [36] F. D. M. Haldane, *Phys. Rev. Lett.* **61**, 2015 (1988).
- [37] N. Goldman, *et. al.*, *Phys. Rev. Lett.* **103**, 035301 (2009).
- [38] Z. Fang, *et. al.*, *Science* **302**, 92 (2003).
- [39] D. A. Abanin, T. Kitagawa, I. Bloch, and E. Demler, *Phys. Rev. Lett.* **110**, 165304 (2013).
- [40] M. Atala, *et. al.*, *Nature Physics* **9**, 795-800 (2013).
- [41] D. Dong-Ling, W. Shengtao, and L.-M. Duan, Arxiv: 1407.1146 (2014).
- [42] G. Wirth, M. Ölschläger, and A. Hemmerich, *Nat. Phys.* **7**, 147 (2011).
- [43] L.-K. Lim, A. Lazarides, A. Hemmerich, and C. M. Smith, *Euro. Phys. Lett.* **88**, 36001 (2009).
- [44] A. Kubasiak, P. Massignan, and M. Lewenstein, *Euro. Phys. Lett.* **92** 46004 (2010).

Supplementary material to "Anomalous Hall effect in ultracold gases"

THE MODEL HAMILTONIAN

We consider an unequal mixture of two-species ultracold fermions (denoted by \uparrow, \downarrow) assuming strong attractive interactions between two species. It is then energetically favorable for fermions to pair, the low energy system is then effectively composed of paired composites and the excess \downarrow fermions. We denote the creation and annihilation operators for \uparrow fermions as $\hat{s}_{\uparrow i}^{\dagger}$ and $\hat{s}_{\uparrow i}$. For the more abundant \downarrow fermions we include both s and p orbitals denoting the corresponding operators as $\hat{s}_{\downarrow i}^{\dagger}$, $\hat{s}_{\downarrow i}$, $\hat{p}_{\downarrow \pm i}^{\dagger}$, $\hat{p}_{\downarrow \pm i}$. In the main text, for simplicity, we have neglected \uparrow -fermion tunneling and all the intra-band tunnelings for \downarrow -fermions from the beginning. Here, let us derive the Hamiltonian without these assumptions and show that, indeed, these effects may be neglected.

The full time-dependent Hamiltonian $H(t)$ consists of three parts $H(t) = H_{\text{tun}} + H_{\text{onsite}} + H_{\text{shaking}}$. The first, H_{tun} describes the tunnelings, H_{onsite} describes the onsite interactions and H_{shaking} describes the shaking. To-

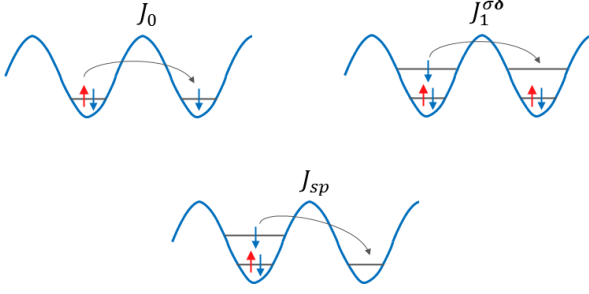


FIG. 4. Pictorial representation of different tunneling processes in Hamiltonian, Eq.(9). The top left panel describes the resonant tunneling process where a \uparrow fermion from a composite tunnel to a neighboring excess \downarrow -fermion occupied site. This tunneling process corresponds to the first term in Hamiltonian H_{tunn} . The top right panel describes the process when an excess fermion can tunnel in the p -band resonantly provided both the sites are already occupied by composites. This reflects the third term in Hamiltonian H_{tunn} . The bottom figure depicts the interaction induced sp tunneling amplitude.

gether they read:

$$\begin{aligned}
H_{\text{tunn}} &= J_0 \sum_{\mathbf{i}, \delta} \hat{s}_{\uparrow\mathbf{i}}^\dagger \hat{s}_{\uparrow\mathbf{i}+\delta} + J_0 \sum_{\mathbf{i}, \delta} \hat{s}_{\downarrow\mathbf{i}}^\dagger \hat{s}_{\downarrow\mathbf{i}+\delta} \\
&+ \sum_{\mathbf{i}, \delta, \sigma} J_1^{\sigma\delta} \hat{p}_{\downarrow\sigma, \mathbf{i}}^\dagger \hat{p}_{\downarrow\sigma, \mathbf{i}+\delta} + \sum_{\mathbf{i}, \delta, \sigma} J_{11}^{\sigma\delta} \hat{p}_{\downarrow\sigma, \mathbf{i}}^\dagger (\hat{n}_{\mathbf{i}}^\uparrow + \hat{n}_{\mathbf{i}+\delta}^\uparrow) \hat{p}_{\downarrow\sigma, \mathbf{i}+\delta} \\
&+ \frac{J_{sp}}{\sqrt{2}} \sum_{\mathbf{i}, \delta, \sigma=\pm} (f_\delta \hat{p}_{\downarrow\sigma, \mathbf{i}}^\dagger \hat{n}_{\mathbf{i}}^\uparrow \hat{s}_{\downarrow\mathbf{i}+\delta} + h.c), \quad (9) \\
H_{\text{onsite}} &= U_2 \sum_{\mathbf{i}} \hat{n}_{\mathbf{i}}^\uparrow \hat{n}_{\mathbf{i}}^\downarrow + U_{01} \sum_{\mathbf{i}, \sigma=\pm} \hat{n}_{\sigma\mathbf{i}}^\downarrow \hat{n}_{\mathbf{i}}^\uparrow + E_1 \sum_{\mathbf{i}, \sigma=\pm} \hat{n}_{\sigma\mathbf{i}}^\downarrow, \\
H_{\text{shaking}} &= \sum_{\mathbf{i}} \mathbf{i} \cdot \mathbf{F}_t (\hat{n}_{\mathbf{s}\mathbf{i}}^\downarrow + \hat{n}_{\uparrow\mathbf{i}}^\downarrow + \hat{n}_{\downarrow\mathbf{i}}^\downarrow + \hat{n}_{\mathbf{s}\mathbf{i}}^\uparrow).
\end{aligned}$$

Here, $\hat{n}_{\mathbf{i}}^{\uparrow(\downarrow)}$, denote number operators of \uparrow (\downarrow) fermions respectively while $\hat{n}_{\pm\mathbf{i}}^\downarrow$ are number operators for the \downarrow p -fermions with \pm -chirality. The same amplitude, J_0 corresponds to the standard tunneling between s orbitals, the corresponding tunneling in the p -band is described by $J_1^{\sigma\delta}$. Moreover, we include density induced (bond-charge) intra-band tunneling for p -orbitals with strength $J_{11}^{\sigma\delta}$. J_{sp} is the amplitude of the hopping between s and p bands which is also induced by the interaction with \uparrow fermions. The various tunneling processes in Hamiltonian (9) are shown in Fig. 4. The tunneling amplitudes

are given by

$$\begin{aligned}
J_0 &= \int \int \mathcal{W}_{\mathbf{i}}^{00}(x, y) H_{\text{latt}} \mathcal{W}_{\mathbf{i}+\delta}^{00}(x, y) dx dy \\
J_1^{\sigma\delta} &= \int \int [\mathcal{W}_{\mathbf{i}}^\sigma(x, y)]^* H_{\text{latt}} \mathcal{W}_{\mathbf{i}+\delta}^\sigma(x, y) dx dy \quad (10) \\
J_{11}^{\sigma\delta} &= g_{2D} \int \int [\mathcal{W}_{\mathbf{i}}^\sigma(x, y)]^* [\mathcal{W}_{\mathbf{i}}^{00}(x, y)]^2 \mathcal{W}_{\mathbf{i}+\delta}^\sigma(x, y) dx dy,
\end{aligned}$$

where $\mathcal{W}_{\mathbf{i}}^{00}(x, y)$ is the Wannier function of the s -band and $\mathcal{W}_{\mathbf{i}}^\sigma(x, y)$ with $\sigma = \pm$ are the Wannier functions corresponding to p_+ - and p_- -bands in the harmonic approximation for the triangular lattice potential. The single particle Hamiltonian for the triangular lattice is denoted by H_{latt} .

Low-energy and resonant subspaces

Now we define the low-energy subspace and the resonant subspace which are coupled by the driving (shaking). First we assume the strong interaction limit i.e. $J_0, J_1^{\sigma\delta}, J_{11}^{\sigma\delta}, J_{sp} \ll U_2, U_{01}$. Yet larger energy scale is set by single particle energy of the p band E_1 and the shaking frequency. Thus we assume $U_2, U_{sp} \ll E_1 \sim \Omega$. $|U_2|$ - the strength of attraction between \uparrow and \downarrow fermions sets the low-energy scale, thus we restrict the analysis to the subspace of Hilbert space where all \uparrow minority fermions are paired with their \downarrow partners. Thus the low-energy local subspace is spanned by $\hat{s}_{\downarrow\mathbf{i}}^\dagger \hat{s}_{\uparrow\mathbf{i}}^\dagger |0\rangle, \hat{s}_{\downarrow\mathbf{i}}^\dagger |0\rangle$ states. As we will show below, due to the sp tunneling and periodic driving this subspace is resonantly connected to the subspace where a paired site can be occupied by p -orbital fermions, $\hat{p}_{\downarrow\sigma, \mathbf{i}}^\dagger \hat{s}_{\downarrow\mathbf{i}}^\dagger \hat{s}_{\uparrow\mathbf{i}}^\dagger |0\rangle$ with energy $E_1 + U_{01}$. Therefore, from now on our Hilbert space will consist of $\hat{s}_{\downarrow\mathbf{i}}^\dagger \hat{s}_{\uparrow\mathbf{i}}^\dagger |0\rangle, \hat{s}_{\downarrow\mathbf{i}}^\dagger |0\rangle, \hat{p}_{\downarrow\sigma, \mathbf{i}}^\dagger \hat{s}_{\downarrow\mathbf{i}}^\dagger \hat{s}_{\uparrow\mathbf{i}}^\dagger |0\rangle$ states.

We now apply the unitary transformation, $\hat{U}_t = \exp[-iH_{\text{onsite}}t - i \int_0^t H_{\text{shaking}}(t') dt']$ transferring the time-dependence in the total Hamiltonian $H(t)$ into the tunneling amplitudes. The new Hamiltonian $H' = \hat{U}^\dagger H \hat{U} - i\hat{U}^\dagger [d_t \hat{U}]$ is given by

$$\begin{aligned}
H' &= J_0 \sum_{\mathbf{i}, \delta} \exp[-iU_2(\hat{n}_{\mathbf{i}}^\downarrow - \hat{n}_{\mathbf{i}+\delta}^\downarrow)t - i\delta \cdot \mathbf{W}_t] \hat{s}_{\uparrow\mathbf{i}}^\dagger \hat{s}_{\uparrow\mathbf{i}+\delta} \\
&+ J_0 \sum_{\mathbf{i}, \delta} \exp[-iU_2(\hat{n}_{\mathbf{i}}^\uparrow - \hat{n}_{\mathbf{i}+\delta}^\uparrow)t - i\delta \cdot \mathbf{W}_t] \hat{s}_{\downarrow\mathbf{i}}^\dagger \hat{s}_{\downarrow\mathbf{i}+\delta} \\
&+ \sum_{\mathbf{i}, \delta, \sigma} \exp[-iU_{01}(\hat{n}_{\mathbf{i}}^\uparrow - \hat{n}_{\mathbf{i}+\delta}^\uparrow)t - i\delta \cdot \mathbf{W}_t] \\
&\times \hat{p}_{\downarrow\sigma, \mathbf{i}}^\dagger \left[J_1^{\sigma\delta} + J_{11}^{\sigma\delta} (\hat{n}_{\mathbf{i}}^\uparrow + \hat{n}_{\mathbf{i}+\delta}^\uparrow) \right] \hat{p}_{\downarrow\sigma, \mathbf{i}+\delta} \quad (11) \\
&+ \frac{J_{sp}}{\sqrt{2}} \sum_{\mathbf{i}, \delta, \sigma=\pm} \exp[-iE_1t - iU_{01}t - i\delta \cdot \mathbf{W}_t] f_\delta \hat{p}_{\downarrow\sigma, \mathbf{i}}^\dagger \hat{n}_{\mathbf{i}}^\uparrow \hat{s}_{\downarrow\mathbf{i}+\delta},
\end{aligned}$$

where $\mathbf{W}_t = \int_0^t \mathbf{F}_{t'} dt'$. We expand the exponential functions in (11) as: $\exp[-i\delta \cdot \mathbf{W}_t] =$

$\sum_n \mathcal{J}_n(K_\delta/\Omega) \exp[-in\Omega t]$. Then as $U_2 \ll \Omega$, after rotating-wave approximation (RWA) and projecting on our local Hilbert space, the first term of Hamiltonian (11) may be resonant only if U_2 contribution vanishes. Since this term corresponds to \uparrow -fermion tunneling (which appear paired only in our subspace) this process is possible only if a paired state and a \downarrow -fermion in s -orbital are neighbours (Fig. 1(a)). Otherwise the pair (composite) is pinned. Similarly, the second term may be resonant ($n_{s\mathbf{i}}^\uparrow = n_{s\mathbf{i}+\delta}^\uparrow = 0$) when a \downarrow -fermion in s -orbital tunnels to a neighboring empty site. The third term gives a resonant contribution via the tunneling process depicted in Fig.4(b). After RWA, all the time-independent tunneling amplitudes of the above intra-band tunnelings are changed by a factor $\mathcal{J}_0(K_\delta/\Omega)$. We see that to minimize the ss and pp tunnelings we have to tune the shaking amplitude such that $\mathcal{J}_0(K_{\delta_0}/\Omega) = 0$ and $\mathcal{J}_0(K_{\delta_-}/\Omega) = 0$. This assures that for the shaking phase $\Phi = 0$, there is no intra-band tunneling along the δ_+ direction as $K_{\delta_+} = K_{\delta_-}$.

In the last term of Hamiltonian (11) the fast oscillation with $E_1 + U_{01}$ frequency must be compensated by appropriate Fourier component yielding the sp resonant condition $E_1 + U_{01} = N\Omega$. Inspecting the tunneling term we see that, the tunneling in p -band is resonantly enhanced only when the composite density in neighboring sites \mathbf{i}

and $\mathbf{i} + \delta$ follows the relation $(n_{\mathbf{i}}^\uparrow - n_{\mathbf{i}+\delta}^\uparrow) = 1$. Due to the type of sp coupling in Hamiltonian, (11), p -fermions may appear only in composite occupied sites. This may occur only from a site occupied by a lonely \downarrow -fermion (if there were a composite at that site, an additional energy difference, U_2 , the pair energy would appear bringing the system out of the chosen resonance). After carrying RWA and in the limit of vanishing intra-band tunneling, the effective Hamiltonian reads,

$$H' = \frac{J_{sp}}{\sqrt{2}} \sum_{\mathbf{i}, \delta, \sigma = \pm} \mathcal{J}_N(K_\delta/\Omega) \exp[-i\sigma \tan^{-1}(\delta_y/\delta_x)] \hat{p}_{\downarrow\sigma, \mathbf{i}}^\dagger \hat{n}_{\mathbf{i}}^\uparrow \hat{s}_{\downarrow\mathbf{i}+\delta},$$

where $\mathcal{J}_N(x)$ defines Bessel function of order- N . We see that, one can control the different tunneling amplitudes by tuning the shaking amplitude, frequency and interaction strength.

When the shaking phase $\Phi \neq 0$, along δ_0 and δ_- directions the intra-band tunneling still vanishes, but remains nonzero along δ_+ direction. Amplitude of the latter can be tuned to values smaller than the sp -tunneling amplitude by changing the interaction strength. Moreover, once the Dice structure of the composites is created, the only possible tunneling along δ_+ direction is the inter-band sp tunneling (compare Fig.1(a) in the main text). So, adding small intra-band tunneling due to a finite shaking phase will not destabilize the Dice structure.